Iranian Journal of Science & Technology, Transaction B, Vol. 28, No. B1
Printed in Islamic Republic of Iran, 2004

DETERMINATION OF EFFECTIVE REFLECTANCE OF SUB SEA OBJECTS IN LANDSAT TM IMAGES: A CASE STUDY OF THE CORAL REEFS OF KHARK AND KHARKOO ISLANDS (NW OF PERSIAN GULF)*

M. MORADI

Marine Geomatics Division, Data Center Department, Iranian National Center for Oceanography
#51, Bozorgmehr Ave., Tehran, 14168, I. R. of Iran
E-mail: moradi@inco.ac.ir

Abstract– The difference between effective reflectance from sub sea objects and water suspended materials is a function of attenuation coefficient (k) of light intensity in bodies of water. The amount of $C\text{-}C_{min}$ (here C is digital number) identifies the effective reflectance and it is possible to differentiate the effective reflectance from sub sea objects and water suspended loads using a specific display image of band ratios. In a ratio display image of Landsat TM band pairs, this difference is a function of $(1- e^{ki})/(1 – e^{kj})$. This value for Khark and Kharkoo sub sea objects (Coral reefs and sandy beds) in the Landsat TM image of 1998 is always positive and less than one. Thus a RGB false color of the atmospherically corrected ratio image of effective reflectance ($C\text{-}C_{min}$) display image as

$$(C – C_{min})_{b2}/(C – C_{min})_{b1} ; (C – C_{min})_{b3}/(C – C_{min})_{b2} ; (C – C_{min})_{b4}/(C – C_{min})_{b3} : (RGB)$$

shows the best separation of the sub sea objects. The proposed model has been used for detecting coral reefs and sandy beds around two Iranian islands in the Persian Gulf, Khark and Kharkoo. The results have been checked by field studies and draft maps, which show a good correlation with a high overall accuracy of about 90%.

Keywords – Landsat TM, Persian Gulf, coral reef, effective reflectance, water suspended material, band ratio

1. INTRODUCTION

Many investigators have shown the value of applying Landsat TM data to mapping the shallow water environment [1-4]. A common mapping technique is to perform a classification on the multispectral data to show sub sea object types [5]. The main problem is that the sub sea objects reflectance is mixed with the effects of the water body depth, suspended materials in the water column and light intensity absorption. Spectral properties for the mapping of water column materials, including suspended sediments [6, 7], algae, chlorophyll [8] and salinity [9] have been well described. These studies generally assume that light radiation falls to the bottom, so sub sea objects reflectances are not considered. The major problem with classification of raw digital numbers is that variations in water depth may alter the spectral characteristics of the sub sea objects. Lyzenga [10, 11] described a technique for removing the influence of depth from spectral data. These studies generally assume that the water body is clear and any reflection is due to sub sea strata materials and are affected by water column body.

In addition, the above-mentioned problems, atmospheric path radiance (back-scatter) and water surface reflectance are added to the effective reflectance emerged from the water body. These additional reflectances are another major problem in interpretation and classification of sub sea objects.

In this paper, the effects of atmosphere, water suspended load and water depth on the reflectance of sub sea habitats are considered, and an applied simple method for mapping the coral reefs and other sub sea objects using Landsat TM data is presented.

*Received by the editors June 15, 2002 and in final revised form January 21, 2003

2. STUDY AREA

Khark and Kharkoo islands are located Northwest of the Persian Gulf (Fig. 1). These two islands are embedded with coral reef communities. In some areas the coral reefs emerge from the water body in low tide. Species and distribution of the coral reefs of Khark and Kharkoo islands have been studied [12, 13]. Bathymetry Charts of this area have been prepared by the Hydrography Department of the National Cartography Center (NCC) of Iran with a scale of 1/50,000 [14]. Bathymetry contour lines overlaid on a Landsat TM false color image of the study area are shown in Fig. 2. Without any enhancement, Fig. 2 also shows the distribution pattern of the water column materials. Note that the distribution of the water column suspended materials and their reflectances have no relation to the water depth. Due to the water discharge of great rivers (such as Karoon, Karkheh, Arvandroud, …) and the direction of the currents in the north-west of the Persian Gulf, a substantial amount of suspended materials are present around these two islands the greater part of the year [15]. Thus, it is impossible to take any images of the clear water condition.

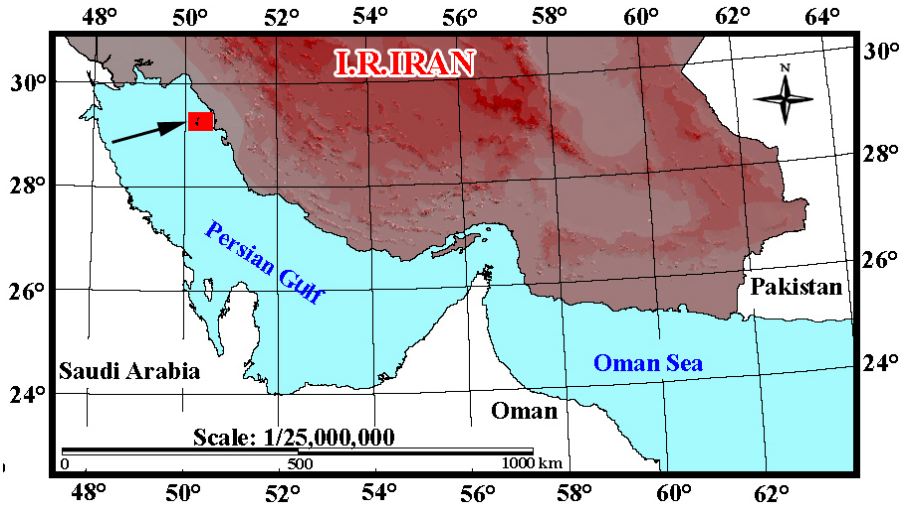

(a)

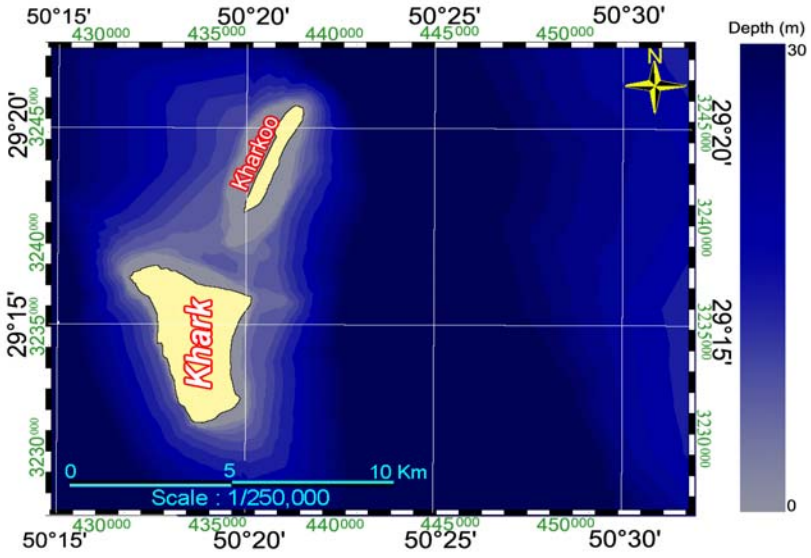

(b)

Fig. 1. a) Location map of study area (filled box), b) Depth variations around Khark and Kharkoo islands

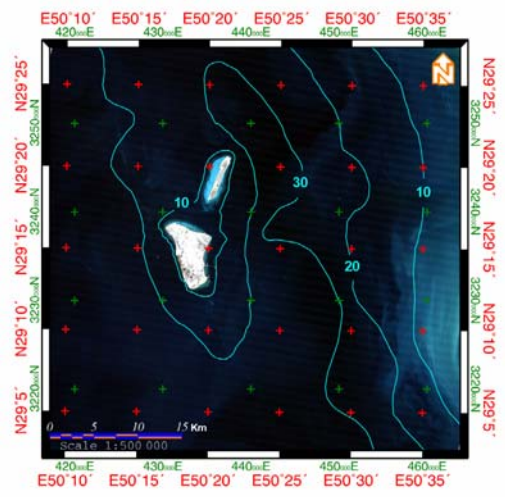

Fig. 2. Bathymetry contour lines overlaid on Landsat TM image of study area, depths are in meter, image display 321: (RGB) [Landsat TM index 164/40, 1998]

3. FACTORS INFLUENCING RADIANCE FROM WATER-MASS

Blue light penetrates up to a maximum of 30m in clear water [16]. When light penetrates water, its intensity decreases exponentially with the increasing depth. Solar radiation must pass through two media, atmosphere and water, before interacting with the sub sea objects and again traversing the same media before reaching the satellite sensors (Fig. 3). Water depth is one of the important factors that control the reflectance of sub sea objects. Also the reflectance of sub sea objects is dependent on the concentration of water suspended materials and sub sea object types. The intensity of the emerged light from the water body is a complex optical interaction of light with parameters, which include [16, 17]

- Sub sea object type
- Concentration of suspended materials in the water column
- Water depth

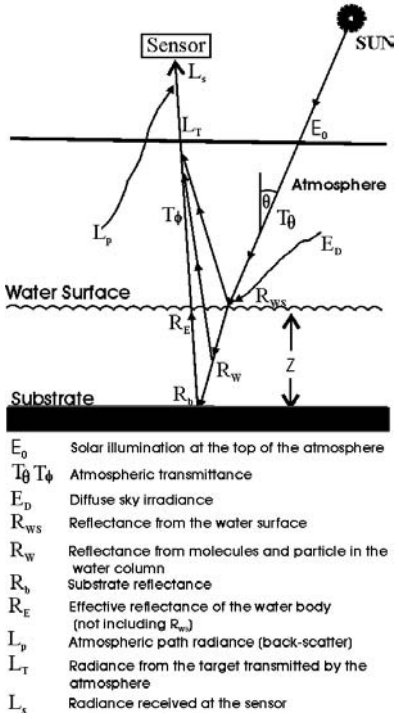

Fig. 3. Radiance path and factors influencing the amount of radiance reaching a sensor over a water-mass [1]

In shallow waters where the concentration of suspended materials is low, the reflectance of the water body is the result of object types, which can be used for bathymetry mapping and/or mapping of sub sea objects. The high concentration of water column suspended materials affects the absorption, scattering and penetration of incident light. In this case the recorded signal by satellite sensor is more than the former, and the resulting data couldn't be used for bathymetry and sub sea objects mapping.

4. REMOVAL OF ATMOSPHERIC SCATTERING EFFECT

The recorded radiance by satellite sensor, $L_{S,}$ is the sum of the radiance directly transmitted from the target, L_T, and the radiance due to atmospheric back-scatter, L_P. Here, atmospheric correction was done based on the "dark pixel subtraction" method, which involves selecting a few numbers of deep-water pixels. Atmospherically corrected reflectance is equal to the average of the apparent reflectance minus twice the standard deviations of deep water reflectance subtracted from all other pixels in each band [18].

5. SEPARATION OF SUB SEA STRATA REFLECTANCE FROM SUSPENDED LOAD REFLECTANCE

Jupp [17] has introduced a generalized formula for the effects of the water body on the sub sea object radiances. Since the reflectance is the ratio of emergent radiance to the total irradiance it is proportional to radiance; Bierwirth *et al*. [19] modified Jupp's formula as below, which relates effective reflectance to water body and sub sea object reflectance

$$R_E = (e^{-2kz})R_b + (1 - e^{-2kz})R_W \quad (1)$$

In a specific band, if the reflectance of the sub sea object is dominant, then

$$R_b >> R_W \quad \text{and} \quad R_E \cong R_b\, e^{-2kz} \quad (2)$$

and if the reflectance of suspended loads is dominate

$$R_W >> R_b \quad \text{and} \quad R_E \cong R_W\,(1 - e^{-2kz}) \quad (3)$$

in all cases

$$R_{b1} > R_{b2} > R_{b3} > R_{b4} \quad \text{and} \quad R_{W1} > R_{W2} > R_{W3} > R_{W4} \quad \text{and} \quad K_1 < K_2 < K_3 < K_4$$

(Numbers refer to Landsat TM band number)

For a specific band pair

$$(R_{Ei}/R_{Ej}) \propto e^{(2z(kj-ki))}\ , \textit{(if dominant reflectance is from the sub sea object)} \quad (4)$$

and

$$(R_{Ei}/R_{Ej}) \propto e^{(2z(kj-ki))}\,((1- e^{ki})/(1- e^{kj})), \quad \textit{(if dominant reflectance is from suspended loads)} \quad (5)$$

Equations (4) and (5) are different in a factor of $(1- e^{ki})/(1- e^{kj})$. This means that in the ratio display image of a Landsat TM band pair, the difference between dominant reflectance from suspended loads or sub sea objects is proportional to $((1- e^{ki})/(1- e^{kj}))$.

The ratio of attenuation coefficient of band pairs is equal to [20]

$$k_i/k_j = a + (a^2 + 1)^{1/2} \quad (6)$$

where $a = (\delta_i - \delta_j) / 2\delta_{ij}$ δ_i is the variance of band i, δ_j is the variance of band j and δ_{ij} is the variance between band i and j. Using this method, the ratio of attenuation coefficient of Landsat TM bands ratio of the study area is calculated and then the value of the fraction $(1- e^{ki})/(1- e^{kj}) = A$ for selected bands ratio is calculated as

$$0.5 < A_{b2/b1} < 0.9, \qquad 0.55 < A_{b3/b2} < 0.75, \qquad 0.25 < A_{b4/b3} < 0.4$$

For all bands, ratio b_i/b_j (where i>j) of bands 1 to 4 Landsat TM of the study area, the value of the fraction $((1-e^{ki})/(1- e^{kj}))$ is always less than one and positive. This means that in the ratio bands display image of the study area, the reflectances of sub sea objects are always greater than the water suspended loads reflectances.

The recorded radiance of a pixel by satellite sensor is equal to the sum of the radiance directly transmitted from the target and the radiance due to atmospheric back-scatter. The radiance of a pixel can be related to the count value, C (i.e. DN) by the equation below [19]

$$L_S = L_T + L_P = CG + L_{min} \tag{7}$$

where G is the instrument gain and L_{min} is the instrument offset

In practice, many other factors influence the amount of radiation recorded at the satellite sensor (Fig. 3). The target radiance, L_T, is equal to the sum of the effective reflectance of the water body, R_E, and the reflectance from the water surface, R_{WS}, and can be given by [19]

$$L_T = (R_E + R_{WS}) TI \tag{8}$$

where I is the total solar irradiance and T is the transmittance of the solar irradiance.

The combination of Eqs. (6) and (7) relates **C** to the reflectance

$$C = R_E (IT/G) + R_{WS} (IT/G) + (L_P – L_{min})/G \tag{9}$$

The radiance emerging from the deep water is the effect of the water body only (R_E=0), and hence

$$C_{min} = R_{WS} (IT/G) + (L_P – L_{min}) /G \tag{10}$$

and

$$C - C_{min} = R_E (IT/G) \tag{11}$$

However, the amount of $C–C_{min}$ Eq. (10) identifies the effective reflectance of the water body. And as discussed above, it is possible to separate effective reflectance from sub sea objects and water suspended loads using the specific ratio image of the study area. Therefore, the ratio display images of the effective reflectance that is based on Eq. (10) are the display image of $C–C_{min}$, and can show the locations of the sub sea objects reflectances. Finally, in an atmospherically corrected ratio display image where R_{WS} is not present, the effective reflectance display image of water body in accordance with Eq. (2) and/or 3 can reveal the sub sea objects locations. As previously discussed, in all ratio display images of b_i/b_j, always i>j (i and j are the Landsat TM bands number). Thus a RGB false color of the atmospherically corrected ratio of effective reflectance (or $C–C_{min}$) display image shows the best separation of the sub sea objects locations. In Fig. 4, the atmospherically corrected RGB false color of

$$(C – C_{min})_{b2}/(C – C_{min})_{b1} ; (C – C_{min})_{b3}/(C – C_{min})_{b2} ; (C – C_{min})_{b4}/(C – C_{min})_{b3} : (RGB) \tag{12}$$

display images have been shown. Sub sea objects which are dominantly sandy bed and coral reef formations have been enhanced in these display images.

(a) (b)

Fig. 4. a) Display image of equation 11 discussed in text of study area. b) Enlarged part image around Khark and Kharkoo islands of Fig. 4-a

6. EVALUATION OF MODEL

The evaluation of the proposed model has been done by a classification of Eq. (11) display image around Khark and Kharkoo islands (Fig. 4b), and the results compared with the sampled training sites, which are collected using the existing maps and field works. Two training site groups of known sandy beds (44 samples) and coral reefs (25 samples) around Kharkoo Island have been sampled and the position of the samples were recorded by GPS in order of 10m accuracy. Because sub sea objects in this area are only sandy beds and coral reef formations, all pixels around Khark and Kharkoo island that represent the reflection from sub sea objects (dark pixels in Fig. 4b), have been classified in two classes using supervised nearest neighborhood method to each training site patch and the land areas have been masked from the image. The classified map has been shown in Fig. 5. The overall accuracy of the classified map was tested using the two training sites explained previously. The confusion matrix of this classification has been shown in Table 1. The overall accuracy of all classified pixels only for sandy beds and coral reefs according to Table 1 is calculated as

$$\text{Overall Accuracy (OA)} = \sum n_{ii} / N$$

where "N" is the number of samples and/or sum of confusion matrix rows or sum of confusion matrix columns that are equal, "n" is the value of the desired cell and i is the row and column index respectively.

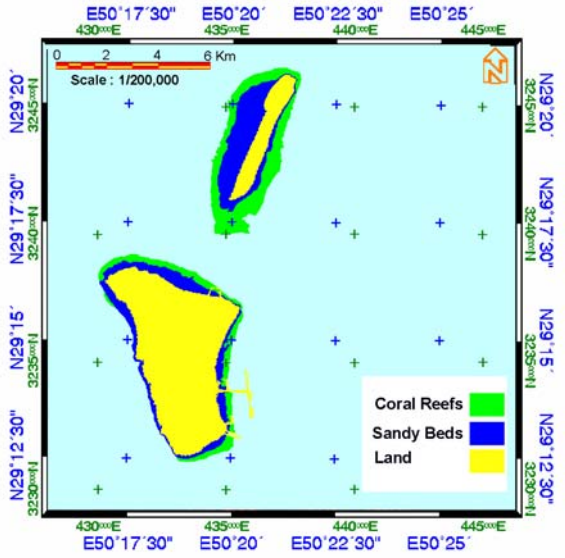

Fig. 5. Classified map of image 4 using supervised nearest neighborhood method showing the distribution of Coral Reef formations and Sandy beds strata around Khark and Kharkoo islands

Table 1. Confusion matrix of classified image (Fig. 6a) for coral reefs and sandy beds (OA=Overall accuracy, n_{ii} = cell ii value, N = Number of samples)

Real Classes / Assigned classes	Coral Reef	Sandy Bed	Sum
Coral Reefs	22	4	26
Sandy Bed	3	40	43
Sum	25	44	69
OA	$= (n_{11} + n_{22})/N = 62/69 = 0.8985$		

However, the overall accuracy of the classified map is equal to 89.85%. All misclassified pixels are situated in the transitional zones between sandy beds and coral reefs, which are narrow and brighter in figure 4b; and the adjacent regions (sandy beds and coral reefs) have been classified correctly.

7. DISCUSSION AND CONCLUSIONS

The modeling described here represents a simple method for processing multispectral data to derive the color of sub sea objects. This method was successfully tested for the Khark and Kharkoo area and its results are compatible with the field surveys. The process represents a valuable tool for the mapping and management of coastal zones.

The correction of illumination and atmospheric back-scatter are essential for applying the model described here. It is proposed that the atmospheric scattering is constant over the scene, and this could be true due to the fact that the study area is relatively small. Therefore the dark pixel subtraction method has been used for atmospheric correction.

In this study, water attenuation coefficients were determined by regressing known bathymetric data against Landsat TM radiances. Because bathymetric data are commonly available in many areas of the Iranian parts of the Persian Gulf, this method of calculating attenuation coefficient can be used. Nevertheless, more work needs to be done both in measuring water attenuation coefficients for various waters, and in developing alternative methods for deriving k_i from remotely sensed data. Water attenuation may also vary within a scene due to the changing concentrations of the water column materials. In this work, water conditions were assumed to be constant over the reefal waters around Khark and Kharkoo islands. This may be a reasonable assumption as the reefal waters around these two islands have been derived from Landsat TM data as clear water.

There are two critical conditions in the interpretation of effective reflectance emerging from the water body. One critical condition is that the effective reflectance is only due to the effects of the water body suspended loads, and the other condition can be assumed for the reflection of sub sea objects. The effective reflectances of these two critical conditions are different from each other as a function of attenuation coefficients of band pairs. Therefore a corrected band pair display image can reveal the effects of these two critical conditions.

In conclusion, the method presented here represents a simple and applicable method for mapping sub sea objects using multispectral data. The important aspect is that the confusing effect of the water depth variations, water suspended materials reflectances and atmospheric scattering must be removed from the spectral nature of the remotely sensed data. This facilitates improved accuracy in the mapping and monitoring of the aquatic environment using remotely sensed data.

Acknowledgements- I offer my sincere thanks to M.Nazarian and S.Fagheeh for editing the manuscript and also to M.R.Shokri for introducing many useful references.

REFERENCES

1. Bullard, R. K. (1983). Detection of marine contours from Landsat film and tape. In: A.P. Cracknell and D. Reidel (Editors), *Remote sensing applications in marine science and technology*. Princeton Univ. Press, Princeton, 373-381.
2. Pirazzoli, P. A. (1985). Bathymetry mapping of coral reefs and atolls from satellite. T*he 5th International Coral Reef Congress* (539-545) Tahiti Int. Univ. Press, Tahiti.
3. Spitzer, D. & Dirks, R. W. J. (1987). Bottom influence on the reflectance of the sea. *International Journal of Remote Sensing, 8*(3), 279-290.
4. Zainal, A. J. M., Dalby, D. H. & Robinson, I. S. (1993). Monitoring marine ecological changes on the east coast of Bahrain with Landsat TM. *Photogrammetric Engineering and Remote Sensing*, *59*(3), 415-421.
5. Clark, C. D., Ripley, H. T., Green, E. P., Edwards, A. J. & Mumby, P. J. (1997). Mapping and measurement of tropical coastal environments with hyperspectral and high spatial resolution data. *International Journal of Remote Sensing*, *18*, 237-242.

6. Curran, P. J. & Novo, E. M. M. (1988). The relationship between suspended sediment concentration and remotely sensed spectral radiance. *Journal of Coastal Research, 4*(3), 351-368.
7. Stumpf, R. P. (1992). Remote sensing of water quality in coastal waters. t*he first Thematic Conference of Remote Sensing for Marine and Coastal Environments* (61-74). New Orleans.
8. Gordon, H. R., Clark, D. K., Mueller, J. L. & Hovis, W. A. (1988). Phytoplankton pigments from the Nimbus-7 coastal zone color scanner: Comparisons with surface measurements. *Science*, *210(*3), 63-66.
9. Khorram, S. (1982). Remote sensing of salinity in the San Francisco Bay delta. *Remote Sensing of Environment*, *12*, 15-22.
10. Lyzenga, D. R. (1978). Passive remote sensing techniques for mapping water depth and bottom features. *Applied Optics*, *17*, 379-383.
11. Lyzenga, D. R. (1981). Remote sensing of bottom reflectance and water attenuation parameters in shallow water using aircraft and Landsat data. *International Journal of Remote Sensing*, *2*(1), 71-82.
12. Pilcher, N. J., Wilson, S., Alhazeem, S. H. & Shokri, M. R. (2000). Status of coral reefs in the Arabian/Persian Gulf and Arabian Sea Region (Middle East). *Int. Conf. of the Status of Coral Reefs of the World* (55-64). Australian Institute of Marine Science, Australia.
13. Vogt, H. P. (1996). Korallenriffe im Persischen Golf: Auswirkungen des Golfkrieges untersucht mittels Unterwasservideoaufnahmen. Ph.D. Thesis, Essen Univ., Essen, Germany.
14. National Cartography Center of Iran (NCC), (1993) Map of Khark and Kharkoo islands. *Map sheet* No. 6148IV-K573, Tehran, Iran.
15. Reynolds, R. M. (1993). Physical oceanography of the Persian Gulf, Strait of Hormuz and the Gulf of Oman-Results from the Mt Mitchell Expedition. *Marine Pollution Bulletin*, *27*, 35-59.
16. Jerlov, N. G. (1976). *Marine optics*. Elsevier, Amsterdam.
17. Jupp, D. L. B. (1988). Background and extensions to depth of penetration (DOP) mapping in shallow coastal waters. *Symposium on Remote Sensing of the Coastal Zone* (2-19). Gold Coast, Queensland.
18. Kaufman, Y. J. (1989). The atmospheric effect on remote sensing and its correction. In: Asrar, G. (Editor), *Theory and applications of optical remote sensing*. John Wiley and Sons Press, UK.
19. Bierwirth, P. N., Lee, T. & Burne, R. V. (1993). Shallow sea-floor reflectance and water depth derived by unmixing multispectral imagery. *Photogrammetric Engineering and Remote Sensing*, *59*(3), 331-338.
20. Maritorena, S. (1996). Remote sensing of the water attenuation in coral reefs: a case study in French Polynesia, *International Journal of Remote Sensing*, *17*(1), 155-166.